Colloids and Surfaces B: Biointerfaces 181 (2019) 437–449

Contents lists available at ScienceDirect

Colloids and Surfaces B: Biointerfaces

journal homepage: www.elsevier.com/locate/colsurfb

Bio-friendly encapsulation of superoxide dismutase into vaterite $CaCO_3$ crystals. Enzyme activity, release mechanism, and perspectives for ophthalmology

Petr V. Binevski[a], Nadezhda G. Balabushevich[a], Viktoria I. Uvarova[a], Anna S. Vikulina[b], Dmitry Volodkin[a,c,*]

[a] Department of Chemistry, Lomonosov Moscow State University, Leninskiye Gory 1-3, 119991 Moscow, Russia
[b] Fraunhofer Institute for Cell Therapy and Immunology, Branch Bioanalytics and Bioprocesses, Am Mühlenberg 13, 14476 Potsdam-Golm, Germany
[c] Nottingham Trent University, School of Science and Technology, Clifton Lane, Nottingham NG11 8NS, UK

ARTICLE INFO

Keywords:
Protein
Recrystallization
Calcite
Sustained release
Ocular drug delivery

ABSTRACT

Mesoporous vaterite $CaCO_3$ crystals are nowadays one of the most popular vectors for loading of fragile biomolecules like proteins due to biocompatibility, high loading capacity, cost effective and simple loading procedures. However, recent studies reported the reduction of bioactivity for protein encapsulation into the crystals in water due to rather high alkaline pH of about 10.3 caused by the crystal hydrolysis. In this study we have investigated how to retain the bioactivity and control the release rate of the enzyme superoxide dismutase (SOD) loaded into the crystals via co-synthesis. SOD is widely used as an antioxidant in ophthalmology and its formulations with high protein content and activity as well as opportunities for a sustained release are highly desirable. Here we demonstrate that SOD co-synthesis can be done at pH 8.5 in a buffer without affecting crystal morphology. The synthesis in the buffer allows reaching the high loading efficiency of 93%, high SOD content (24 versus 15 w/w % for the synthesis in water), and order of magnitude higher activity compared to the synthesis in water. The enormous SOD concentration into crystals of 10^{-2} M is caused by the entrapment of SOD aggregates into the crystal pores. The SOD released from crystals at physiologically relevant ionic strength fully retains its bioactivity. As found by fitting the release profiles using zero-order and Baker-Lonsdale models, the SOD release mechanism is governed by both the SOD aggregate dissolution and by the diffusion of SOD molecules thorough the crystal pores. The latest process contributes more in case of the co-synthesis in the buffer because at higher pH (co-synthesis in water) the unfolded SOD molecules aggregate stronger. The release is bimodal with a burst (ca 30%) followed by a sustained release and a complete release due to the recrystallization of vaterite crystals to non-porous calcite crystals. The mechanism of SOD loading into and release from the crystals as well as perspectives for the use of the crystals for SOD delivery in ophthalmology are discussed. We believe that together with a fundamental understanding of the vaterite-based protein encapsulation and protein release, this study will help to establish a power platform for a mild and effective encapsulation of fragile biomolecules like proteins at bio-friendly conditions.

1. Introduction

The eye is rather an isolated organ, and the pathological processes within it are preferably treated not via systemic but by local drug intake. Many drugs for the treatment of eye diseases are used in the form of eye drops. However, only 1–5% of the drug penetrates the cornea through the internal structures of the eye [1]. After instillation, a rapid and large loss of the drug occurs due to its flushing from the surface of the eye with a tear and with blinking [2]. To get into the internal structures of the eye, the drug must penetrate through the cornea, where the epithelium of the cornea is the most difficult barrier to overcome. Densely packed cells of multilayered epithelium work as a selective barrier for low-molecular-weight substances and prevent the diffusion of macromolecules. The duration of contact of the drug with the cornea is usually 5–25 min [3], which greatly limits the effectiveness of the action of aqueous solutions of drugs.

In the last 20 years, more and more works have appeared, in which it is proposed to use more efficient systems for the delivery of

* Corresponding author at: Nottingham Trent University, School of Science and Technology, Clifton Lane, Nottingham NG11 8NS, UK.
E-mail address: dmitry.volodkin@ntu.ac.uk (D. Volodkin).

https://doi.org/10.1016/j.colsurfb.2019.05.077
Received 4 March 2019; Received in revised form 22 May 2019; Accepted 30 May 2019
Available online 31 May 2019

ophthalmic drugs to the eye. These include, first and foremost, the use of drug complexes with cyclodextrins [4], the combined use of ophthalmic drugs with agents that enhance the penetration of drugs through biological membranes (EDTA, taurocholic and capric acids) [5], the use of polymer gels [6], colloidal systems containing a drug immobilized on a carrier. The latter include systems with drugs embedded in liposomes [7] and nanoparticles of different nature [8]. Despite of significant advancements in ocular drug delivery, low duration of the contact of drug delivery systems with the cornea remains challengeable. One of the promising strategies is the use of mucoadhesive systems for which the residence time of the drug carriers is governed not by tear but by mucus turnover; hence drug retention is substantially improved [9].

From the other hand, in the recent years growing demand on the biopharmaceuticals used for the treatment of indications in the eyes has emerged. Mainly, this is because ophthalmic macromolecular drugs often allow for effective therapy with fewer side effects [10].

The gap between the discovery of modern macromolecular drugs and their utilization for ophthalmological applications is largely created by the lack of proper drug delivery technologies because nearly all existing ocular delivery systems have been tailored for the small molecules. This provokes the urgent need of the development of drug delivery systems suitable for macromolecular therapy [10], e.g. employing promising ophthalmological protein superoxide dismutase (SOD).

The enzyme SOD has attracted an attention of scientists since the middle of the twentieth century. Dismutation of an oxygen radical into hydrogen peroxide with SOD is often called primary protection, since this enzyme prevents the formation of free radicals. Antioxidants, SOD in particular, are known to be beneficial in the treatment of various diseases related to an oxidative stress. Thus, SOD was reported to reduce inflammation [11], accelerate the healing of skin lesions caused by burns, systemic lupus erythematosus, and herpes [12–14], protect cultured human neurons under oxidative stress [15], reduce ischemia-reperfusion injury [16–18], inhibit angiotensin II intra-neuronal signaling [19], prolong viability of β-cells [20], be effective in the treatment of rat adjuvant arthritis [21], etc.

One of the possible applications of SOD is the treatment of the various eye diseases associated with oxidative stress. Thus, SOD was used for the treatment of lens-induced and bovine albumin-induced uveitis in rabbits [22,23], as well as for the treatment of acute corneal inflammation in animals induced by sodium hydroxide [24,25]. SOD was employed for the treatment of severe experimental allergic uveitis induced by retinal S antigen in rats [26], while poly(ethylene glycol)-(PEG-) modified SOD was employed for the treatment of the same type of uveitis in guinea pigs [27].

When systemically administered, SOD significantly loses its activity due to the influence of proteolytic enzymes and is rapidly eliminated from the circulatory system through the kidneys [28–30]. In the recent years, a significant amount of research aimed at the increase of the bioavailability of SOD for both systemic and local administration. Various methods of SOD modification are used to protect the enzyme against adverse environmental effects, to prolong the release and achieve the targeted delivery. These methods include: chemical modification (PEGylation [31], binding to lecithin [32]), inclusion in liposomes [33], as well as micro- and nano-encapsulation of the enzyme [18,34–36], enzyme immobilization using the layer-by-layer assembly [37].

Cheap, biocompatible and biodegradable $CaCO_3$ micro- and nanocrystals are widely used in the field of encapsulation as matrices for assembly of polymer-based carriers as well as containers for the inclusion of various drugs [38–47]. Special attention is paid to the vaterite modification of $CaCO_3$. Vaterite crystals can easily be synthetized in laboratory and typically represent spherical particles with a controlled size from hundreds of nanometres to tens of micrometres [43]. Moreover, not only the dimensions of the crystals but also a shape [48] and the internal porosity [49] can be adjusted. The highly porous surface of the vaterite crystals allows the inclusion of significant amounts of biologically active substances, including labile proteins and enzymes [38,39]. A number of approaches including co-synthesis, infiltration, and solvent exchange have been introduced for the loading of proteins into the vaterite crystals in order to form protein-based nano- and micro-particles [50–52]. In addition, the crystals have been reported as effective carriers for diagnostics, e.g. using Raman spectroscopy [53,54] and external manipulation [55], as sacrificial templates to assemble polymer-based functional structures from multilayers [56] and from other functional molecules such as PEG and poly-*N*-isopropylacrylamide [57,58]. The crystals can take multiple roles being not only sacrificial templates utilized to formulate polymer particles with a well-defined structure, but also can serve as a source of calcium and as porogens to assemble alginate gels with a tuned internal porosity and encapsulated molecules of interest such as proteins [59,60].

The introduction of proteins and enzymes during the formation of vaterite crystals (co-synthesis) allows to achieve a high inclusion, much exceeding the inclusion when adsorbed on the surface of preformed crystals [30,44,61–69]. However, due to alkaline conditions during the co-synthesis (pH more than 10), labile proteins and enzymes can significantly lose their bio-activity [70].

In the study [36], alginate granules were obtained, including those based on vaterite microcrystals containing SOD and inhibitors of proteolytic enzymes. The model system shows the possibility of utilizing such a system for oral use and protection from the action of proteolytic enzymes. However, the features of the interaction of SOD with vaterite microcrystals, the preservation of the enzyme activity and the mechanism of SOD release from crystals have not been investigated.

In addition to the obvious advantages, most of the aforementioned carriers have a number of disadvantages including the complexity of the synthesis, the high costs for the synthesis, and a potential toxic effect of the carrier. Calcium carbonate microcrystals are deprived of these disadvantages. In addition, high mucoadhesiveness of vaterite microcrystals which has recently been demonstrated in [69] and [71] might promote the retention of the microcrystals in the eye due to the binding to the ocular mucus. Simplicity of the synthesis, mild synthesis and mild crystal decomposition conditions, a large specific surface area – all this makes the crystals as perfect carriers for ophthalmic drugs in general and for SOD in particular.

In this work we investigate whether SOD can effectively be encapsulated into the vaterite crystals keeping its bioactivity and offering controlled release opportunities. For that we investigated the loading of the SOD in water and in the buffer (final pH 8.4) and compared the loading performance by the analysis of thermodynamic parameters of the encapsulation process, polymorph phase of the crystals formed as well as SOD bioactivity retention and the release of SOD at physiologically relevant ionic strength. Using modern techniques and approaches we conclude about the SOD loading and release mechanisms. This study is indispensable for getting fundamental knowledge on encapsulation and controlled release of proteins and other bioactive fragile biomolecules employing the vaterite $CaCO_3$ crystals.

2. Experimental section

2.1. Materials

$CaCl_2$ 99% was purchased from «Biomedicals» ICN, Inc. (USA); Na_2CO_3 99.8% was purchased from «Pharma» (Russia); recombinant human superoxide dismutase-1 was purchased from «Enzyme Technology» (Russia); TRIS, NaCl 99% and Coomassie Brilliant Blue G-250 were purchased from «Sigma-Aldrich (USA); EDTA was purchased from «Reakhim» (Russia). Other chemicals were all purchased from «Sigma», Germany. All chemicals used in this study were of analytical grade and used without purification. Ultrapure water was used for all experiments.

2.2. Preparation of the SOD-loaded $CaCO_3$ crystals

The co-synthesis method [68] with some modifications was employed to encapsulate the SOD into the crystals. Before use, all salt solutions were filtered (RC 0.20 mm filter, Corning Inc., USA). Briefly, 1 ml of 1 M $CaCl_2$ was added to 3 ml of solution with dissolved SOD (in water or in 100 mM TRIS-buffer with pH 7.5) to achieve the desired protein concentration in the mixture of 0.5–6 mg/ml and final buffer concentration of 60 mM. The concentration of the TRIS buffer was used as per above, if not specifically mentioned. 1 ml of 1 M Na_2CO_3 solution was rapidly added and the mixture under agitation on a magnetic stirrer (400 rpm) at room temperature for 45 s. After that, the agitation was stopped, and the reaction mixture was left without stirring for 15 min, allowing preformed amorphous primary precipitates of $CaCO_3$ to transform slowly into vaterite crystals. Finally, the supernatant was discarded, 5 ml of deionized water was added to the pellet, stirred and after 15 min incubation the washing solution was removed. This washing procedure was repeated twice. The precipitated $CaCO_3$ microcrystals were lyophilized and stored in a closed container. Empty crystals (without SOD) were prepared in using the same protocol and solutions but without SOD.

2.3. Determination of protein content

Using a UV spectrophotometer (Cary 50 Conc, «Varian», USA), two independent methods were carried out to determine the SOD concentration: the Bradford protein assay [72] and the measurement of the optical density of the SOD at a wavelength of 280 nm. All measurements were performed in triplicates. To determine the protein loading efficiency into the crystals, the loaded SOD amount was calculated from the total amount of added enzyme and that measured in the supernatant of the crystals after preparation and the washing steps.

2.4. Assessment of the enzyme biological activity

To determine the specific enzymatic activity of recombinant human superoxide dismutase an inhibition of autoxidation SOD reaction by pyrogallol [73] was assessed. The SOD-containing solution (native SOD solution or the solution obtained after dissolution of $CaCO_3$ crystals in 200 mM EDTA) was diluted with water by the dilution factor from 10 to 4000. 20 µl of the obtained solution was added into a well. Further, 160 µl of 50 mM TRIS, pH 8.2, containing 1.25 mM DTPA, were added. Pyrogallol was first dissolved in acetone to a final concentration of 5 mg/ml and diluted ten times with water immediately before the measurement. The reaction was initiated by addition of 20 µl of the pyrogallol solution. The mixture was rapidly stirred and the optical density was measured at 420 nm for 5 min. 180 µl of 50 mM TRIS, pH 8.2, containing 1.25 mM DTPA, with 20 µl of pyrogallol was used as control. The measurements were carried out on a microplate reader Infinite M200, «Tecan», Switzerland.

2.5. Protein adsorption

The adsorption isotherms for SOD loading into the crystals by co-synthesis in water or in the TRIS buffer were constructed and the thermodynamic parameters of the adsorption process were calculated. The initial SOD concentration (C_0) ranged from 0.5 mg/ml to 6 mg/ml. Equilibrium protein concentrations (C_e, mg/ml) were determined from the loading efficiency. To determine the adsorption equilibrium constants, the Langmuir adsorption isotherm model was used [68]. To calculate the input values of adsorption and the adsorption equilibrium constant, the experimental isotherms were linearized by plotting the C_e vs C_e/q_e.

2.6. Synthesis of FITC-labeled SOD

To a solution of 2 mg/ml SOD in 0.5 M carbonate buffer, pH 9, a solution of 0.1 M FITC in carbonate buffer, pH 9, was added dropwise with constant stirring until the protein:FITC molar ratio was adjusted to be 1:2. The resulting solution was incubated for 4 h in a darkness, and then dialyzed twice against 50 mM TRIS, pH 7.0.

2.7. Confocal laser scanning microscopy (CLSM)

The dried crystals were placed in water and transferred to a glass Petri dish and further examined on a Nikon Eclipse Ti-E CLSM microscope with the confocal module A1 (Nikon Corporation, Japan). 488 nm wavelength of the laser and an Apo TIRF 60x/1.49 oil lens were used. The fluorescence has been measured in the wavelength range of 500–550 nm. A series of optical sections were obtained and a three-dimensional reconstruction was performed (horizontal projection of the optical sections on the plane). The images were analyzed by the Nis-Elements program and also using the ImageJ to obtain the fluorescence profile.

2.8. Scanning electron microscopy (SEM)

The surface structure of particles and their shapes were studied by SEM using LEO SUPRA 50 VP (Germany) with the VPSE detector. The optimum acceleration voltage was chosen at 20–21 kV, the 4th scanning speed was used, and the noise was removed by integration along the line. To carry out the experiment, the crystals were previously lyophilized and placed on the adhesive tape.

2.9. X-ray diffraction analysis

X-ray experiments were performed on a diffractometer with a rotating anode Rigaku D/MAX 2500 (Rigaku, Japan) in the reflection mode (Bragg-Brentano geometry) using Cu K_α radiation and a graphite monochromator. Parameters of the X-ray generator in the experiment are: accelerating voltage 50 kV, cathode heating current 250 mA (total power of the X-ray tube is 12.5 kW). Alignment of the optical scheme of the diffractometer and adjustment of the parameters of the discriminator amplifier were carried out automatically under the control of the diffractometer software. The diffraction patterns for phase analysis at room temperature were taken in quartz cuvettes using a standard sample holder. The spectrum was collected in a continuous θ–2θ scanning mode with a detector speed of 3°/min and averaging parameter of 0.02° on a 2θ scale. The shooting interval was from 15 to 70° on a scale of 2θ. To determine the parameters of a unit cell, the survey was conducted using an internal standard (germanium). The data was processed using the Winxpow software package and the ICDD PDF 2 database.

2.10. In vitro release of SOD

In a standard protocol, 10 mg of the dried crystals with co-synthesized SOD were dispersed in 1 mL of a 150 mM NaCl solution, then the suspensions were incubated for various time intervals (10–200 min, 24, 36 h) at room temperature. After the incubation, the suspensions were centrifuged at 9000 rpm for 5 min, and the SOD concentration and activity were determined in the supernatant. All experiments were performed in triplicates.

2.11. Dynamic light scattering (DLS) measurements

The average hydrodynamic diameter and polydispersity index were measured by DLS using a Zetasizer Nano ZS instrument (Malvern Co., Ltd., UK). The measurements were carried out at a fixed angle of 90° at 25 °C repeatedly to obtain statistically reliable results. The data was

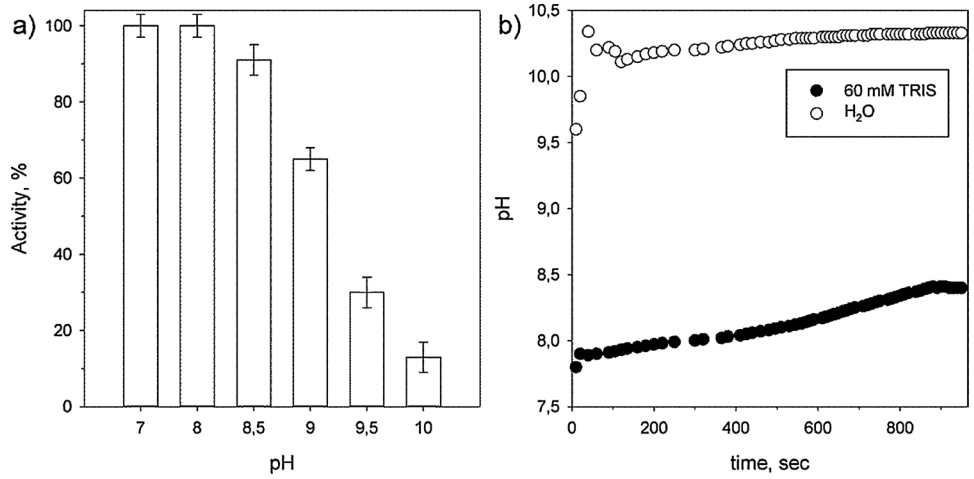

Fig. 1. (a) The residual SOD biological activity after 1 h incubation in 0.1 M TRIS with pH values ranging from 7 to 10. Protein concentration 1 mg/ml. (b) The evolution of the pH in the working medium during synthesis of vaterite $CaCO_3$ crystals in water and in TRIS buffer.

automatically processed using Zetasizer v.7.03 software.

3. Results and discussion

3.1. Optimization of vaterite crystal synthesis

Our preliminary studies demonstrated that the activity of SOD (32 kDa, pI 4.5), significantly decreases when the enzyme is incubated in TRIS buffer solution with the pH above 8.5 (Fig. 1a). At pH 8.5 the activity retention is about 90%, whereas at pH 9.5 the only 30% is retained. Therefore, in order to preserve the activity of the enzyme, the preparation of vaterite crystals, by the standard mixing of $CaCl_2$ and Na_2CO_3 solutions, should be carried out at pH below 8.5.

In accordance with Lewis theory of acids and bases, $CaCO_3$ is a typical conjugate base and is prone to a partial hydrolysis in aqueous solution and has a pKa of about 9. Vaterite $CaCO_3$ has solubility in water of about $1.3{\cdot}10^{-5}$ M, and therefore crystal hydrolysis results in an elevated pH value of aqueous suspension of $CaCO_3$ crystals. As a result, under standard crystal synthesis in water, the pH of the suspension rapidly increases to a value more than 10, reaching a final value of 10.3 (Fig. 1b).

A simple option to keep the pH constant during the synthesis process is to perform the synthesis in a buffer (usually the synthesis is done in water). First we have assessed the variation of pH value during the synthesis when the synthesis has been performed in 60 mM TRIS buffer, pH 7.5. As it can be seen from Fig. 1b, under these conditions, the pH of the medium increases during the formation of the vaterite microcrystals, but did not exceed 8.5, reaching a final pH of about 8.4.

In order to understand whether the presence of the TRIS buffer during the crystal synthesis can affect the crystals properties, the crystal morphology has been tested. The crystal size has not been significantly affected by the presence of the buffer. The average diameter of the crystals prepared in water and in the TRIS buffer are 3.8 ± 0.3 μm and 3.4 ± 0.5 μm, respectively. In order to probe an effect of the TRIS buffer on the crystal morphology, the crystals have been prepared in the presence of high concentration of the buffer, i.e. in 120 mM TRIS buffer with the same pH. SEM images of the crystals prepared in water and in the buffer are shown in Fig. 2a and b, respectively. The crystals look rather similar, however, the surface morphology can only be assessed by a deep look. Enlarged images of the crystal surface are presented in Fig. 2c,d. The morphology represents a channel-like structure with the channel width (D) to be defined according to the the designated lines in the enlarged images. The average values of the channel widths for the crystals prepared in water and the buffer have been found to be 33 ± 9 nm and 37 ± 7 nm, respectively. These values are not statistically different proving that the presence of the TRIS buffer does not affect the surface morphology of the crystals. Based on the main results of in the study [49], the external morphology of the crystals scales with pores in the internal volume of the crystals. This allows one to assume that the internal structure of vaterite crystals (porosity) is not influenced by the presence of the TRIS buffer. This gives a good option for the synthesis of vaterite crystals in TRIS buffer at the final pH 8.4, that to some extent exceed the physiological pH value, however, is by much fare away from the alkaline pH 10.3 as for the synthesis in water.

To further test whether the TRIS buffer can affect the internal structure of the crystals, the X-ray diffraction analysis has been performed. This analysis allows to identify the polymorph form of the $CaCO_3$, i.e. the porous spherical vaterite and non-porous cubic calcite forms (Fig. 3, top). According to the results of the X-ray analysis (Fig. 3, bottom), the presence of the TRIS buffer did not lead to an increase in the calcite content, and the content of the vaterite was not less than 90%. This corresponds to a rather small number of calcite crystals prepared during the synthesis, however, the majority of the crystals obtained belong to the vaterite polymorph.

3.2. Loading of SOD into crystals

The preparation of vaterite crystals with SOD was carried out in 60 mM TRIS buffer or in water to have final pH of 8.4 and 10.3, respectively. For that, SOD was pre-mixed with a solution of $CaCl_2$, and then a solution of Na_2CO_3 was added. The concentration of SOD in the suspension was varied from 0.1 to 6 mg/ml. Even at a high concentration of the enzyme, no change in the phase composition of the crystals was observed (no increased content of calcite was present, data not shown).

CLSM analysis demonstrated rather homogeneous distribution of SOD-FITC co-synthetized in the vaterite crystals (Fig. 4). It is hard to make qualitative conclusions regarding a real distribution of the enzyme into crystals because of potential optical effects associated with the penetration of a light into porous vaterite crystals. However, a strong fluorescence from the whole volume of the crystal (Fig. 4c) can only indicate that the crystal is likely uniformly loaded with the SOD.

No sterical difficulties can be expected for the diffusion of SOD molecules into pores of the crystals (typical pore sizes are in the range 5–30 nm [68]). According to the DLS data (Fig. 5a,b), the size of the SOD molecule in water and in the TRIS buffer is about 6 nm, so the enzyme is able to penetrate into the pores of crystals. At the same time, the uptake of SOD via the co-synthesis may have a mechanism that does not involve a direct diffusion of SOD through the pores but may be based on the embedding of SOD molecules during the crystal growth. In

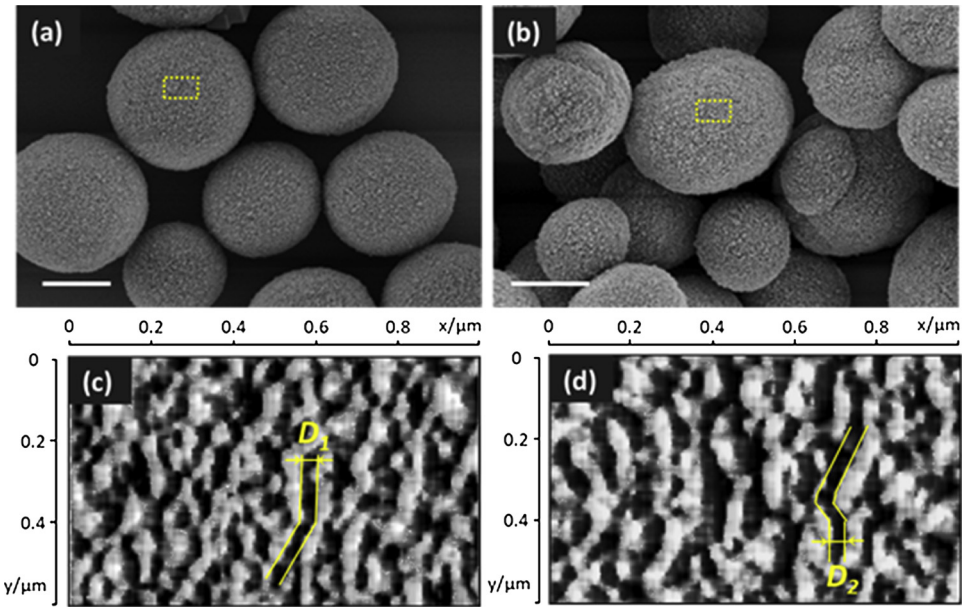

Fig. 2. SEM images of $CaCO_3$ microcrystals prepared in water at pH 10.3 (a) and in 0.2 M TRIS-buffer at pH 8.2 (b). Scale bars are 1 μm. (c) and (d): top views on surface areas inside the designated rectangles in (a) and (b), respectively. Pore diameters (D_1 and D_2) have been estimated as illustrated in (c) and (d), respectively. $D_1 = 33 \pm 9$ nm (n = 40) and $D_2 = 37 \pm 7$ nm (n = 40) are statistically not different.

order to better understand the loading mechanism, the thermodynamic parameters have been extracted from the adsorption isotherms constructed for the SOD co-synthesis as discussed below.

The effect of SOD concentration on the inclusion in microcrystals in water and in the TRIS buffer has been studied (Fig. 6). After the determination of the protein concentration in the supernatants, the amount of SOD in the crystals was calculated and referred to the total amount of the enzyme in order to work out the encapsulation efficiency. As it can be seen from Fig. 6a, with the increase of the protein concentration from 0.5 to 6 mg/ml, the encapsulation efficiency decreased from 92 to 35% and from 93 to 52% for synthesis in water and in TRIS buffer, respectively. This trend collaborates well with the one observed for the co-precipitation of other proteins (e.g. [70]) and can be explained by the saturation of the microcrystals. These results demonstrate high efficiency (up to 93%) to uptake the SOD from the solution by the co-synthesis.

Taking into account the amount of the protein in the crystals and the mass of $CaCO_3$ after the synthesis, the adsorption isotherms for the SOD were calculated by plotting the equilibrium adsorption capacity (q_e) against the equilibrium SOD concentration C_e (Fig. 6b). As in our previous studies [68], for the analysis of isotherms, the adsorption equilibrium constants were determined using the Langmuir monolayer adsorption model:

$$q_e = \frac{q_m K_a C_e}{1 + K_a C_e} \quad (1)$$

where q_e is the equilibrium adsorption, mg/g $CaCO_3$; C_e – equilibrium protein concentration, mg/ml; q_m – maximum adsorption capacity of the crystals for SOD, mg/g; K_a – equilibrium constant, ml/mg.

The thermodynamic parameters were extracted after presenting the equation above as C_e vs C_e/q_e as shown in the Table 1.

The maximum adsorption capacity of the crystals for SOD for the synthesis in the TRIS buffer was more than 50% times higher than that obtained for the synthesis in water (240 and 150 mg of SOD per g of $CaCO_3$, respectively). The concentration of the SOD in crystals achieved by the synthesis in the buffer is about 1.6 times higher than the maximum adsorption capacity, i.e. 380 mg/ml (or ca 10^{-2} M), taking into account that the density of vaterite is 1.6 g/cm^3 [39]. This extremely high concentration (about a third of the concentration of SOD in a pure solid SOD) can only be explained by an aggregation of SOD molecules inside the crystal. Very high loading has previously been observed for catalase loading into the crystals via co-synthesis [68] that has been driven by Ca^{2+}-mediated catalase aggregation during the first step of the co-synthesis procedure (catalase mixing with $CaCl_2$). The SOD has a strong tendency to aggregate in the presence of calcium ions [74] and we assume that it is embedded into the crystals in the aggregated state.

While the intermolecular interactions between SOD molecules explain well the high loading capacity of vaterite microcrystals in respect to SOD in general, the pronounced difference between the co-synthesis in TRIS buffer and in water can be explained from the point of view of electrostatic attraction. Apparently, this high loading in the buffer was likely facilitated by stronger electrostatic interactions between the negatively charged SOD (pI 4.5) and the microcrystals that have a greater positive surface charge at a lower pH according to the following study [75]. At the same time, the reciprocal of the adsorption equilibrium constant, corresponding to the equilibrium concentration when $q = q_m/2$, had a higher value for the loading in TRIS buffer. This (as can obviously be concluded from the comparison of K_a) indicates a low strength of binding of SOD to the crystals in the presence of TRIS compared to the synthesis in water. At the same time, the q_m is significantly higher for the synthesis in TRIS (Table 1). This can be explained by a formation of multilayers of SOD (SOD aggregates) during the loading into the crystals. This will result in a deviation from the Langmuir model (assumes a monolayer formation). However, this can be explained as the following: the more SOD is adsorbed forming an aggregate, the less strong is the formation of new SOD layers assuming that the SOD-crystal interaction is stronger compared to the SOD-SOD one. An alternative adsorption model for the SOD loading has not been used here due to a good fitting to the Langmuir model and a typical profile of the adsorption isotherm obtained for the Langmuir adsorption phenomenon. However, as described above, the deviation from the Langmuir model can take place.

The Gibbs energy for the SOD co-synthesis was calculated using the equation:

$$\Delta G = -RT \ln K_a \quad (2)$$

where R is the universal gas constant, 8.31 m^2 × kg × s^{-2} × K^{-1} × J/(mol × K^{-1}); T is the temperature, K; K_a – equilibrium constant, M^{-1}.

The negative values of the Gibbs energy change for the co-synthesis in water and in the TRIS buffer show a significant shift in the equilibrium towards SOD adsorption. These values are lower compared to those obtained for the co-synthesis of the protein catalase. [68] From the other side, the K_a values for the co-synthesis of SOD in water (K_a in this study is ca 10^4 M) is almost two orders of magnitude lower than

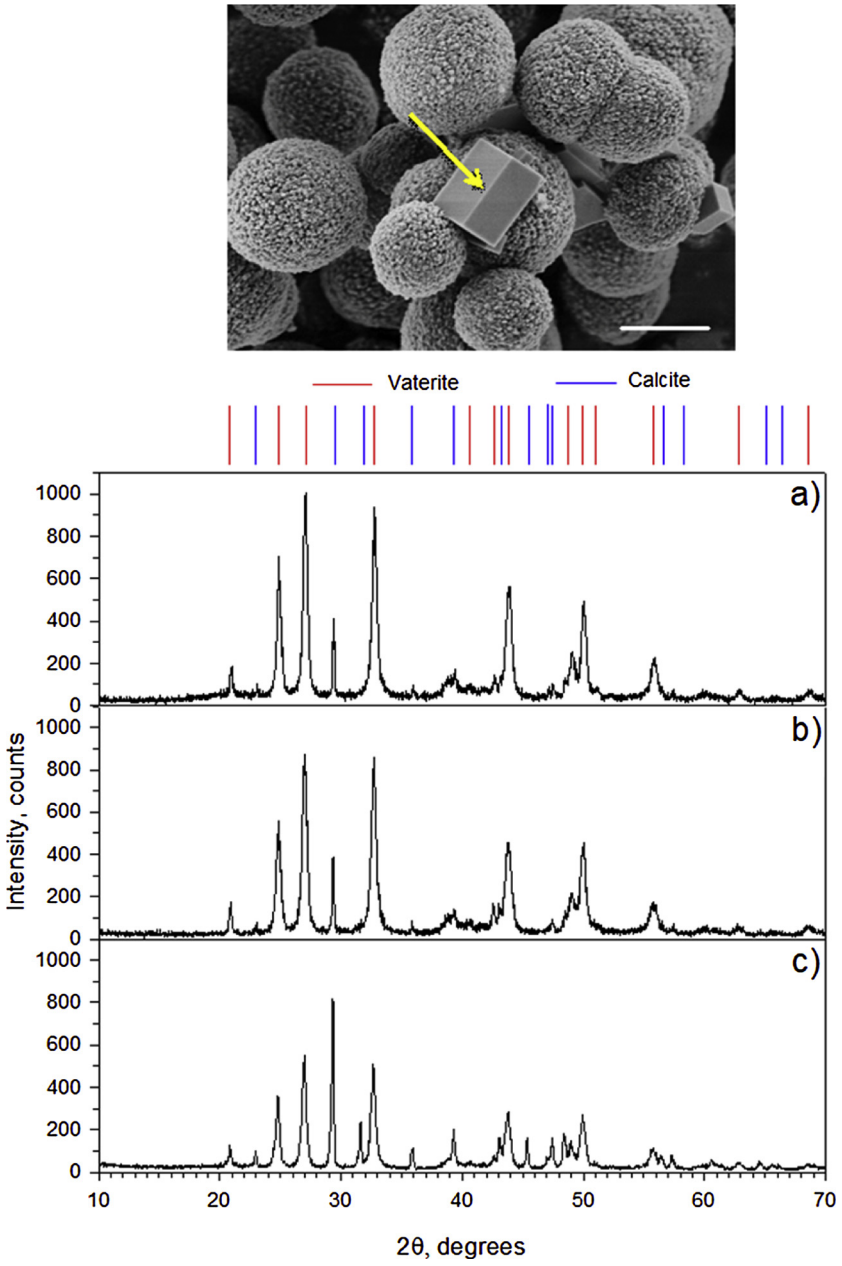

Fig. 3. (top) SEM image of $CaCO_3$ crystals prepared in water demonstrates a porous nature of spherical vaterite crystals and non-porous calcite crystal (depicted with an arrow). The scale bar is 2 µm. (bottom) XRD spectra for crystals prepared in water (a) and in TRIS buffer (b) as well as the SOD-containing crystals after 24 h of incubation in 150 mM NaCl; SOD loading concentration 1 mg/ml (c). (For interpretation of the references to colour in the text, the reader is referred to the web version of this article.)

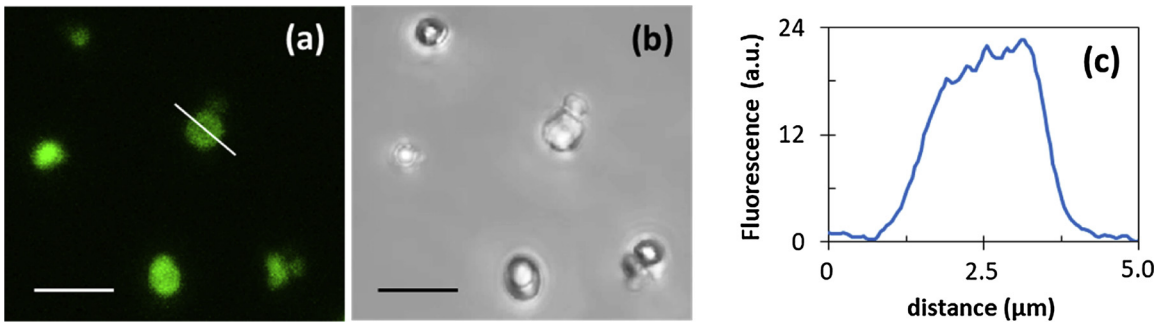

Fig. 4. Fluorescence (a) and light transmittance (b) CLSM images of vaterite $CaCO_3$ crystals with co-synthetized SOD-FITC. SOD loading concentration 1 mg/ml. Scale bars are 5 µm. Fluorescence profile (c) is taken across the white line taken in (a). Background fluorescence is subtracted to get the fluorescence profile.

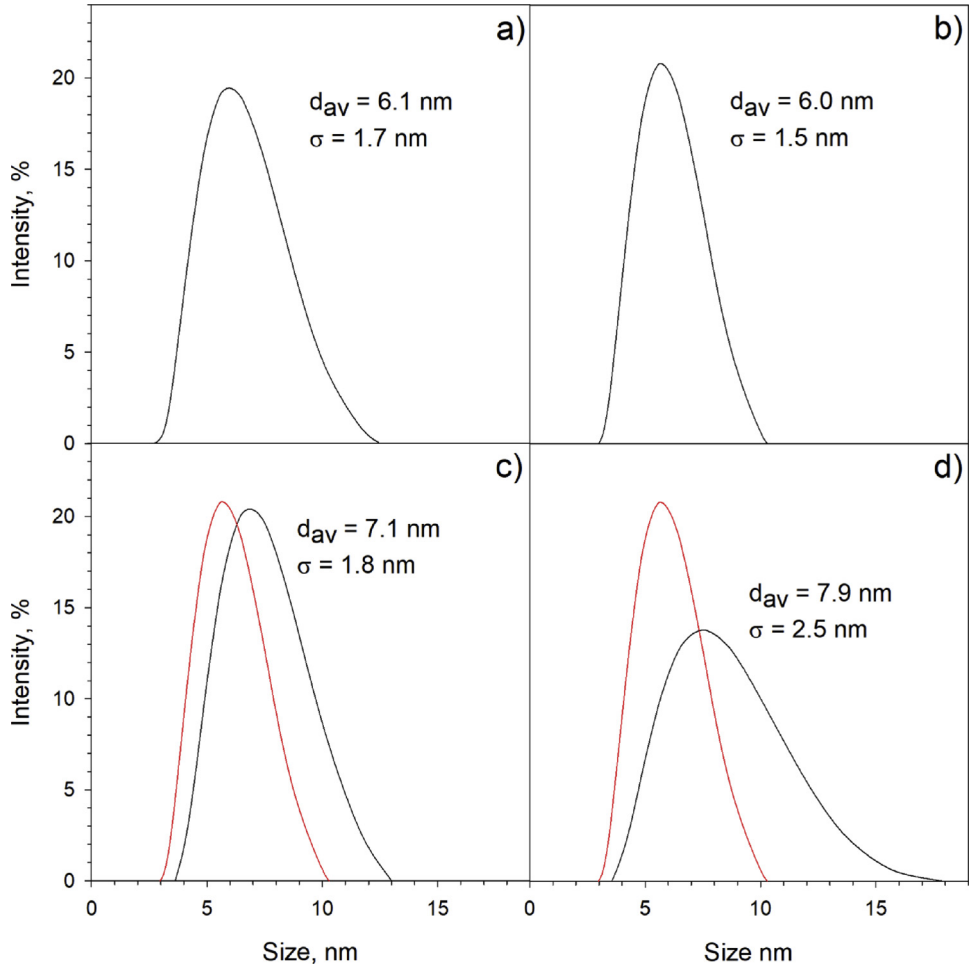

Fig. 5. DLS intensity weighted distribution of SOD hydrodynamic diameters for the SOD in water (a) and in 0.1 M TRIS buffer (b) as well as SOD released from the crystals after 10 min (c) and 24 h (d) of incubation (the left spectra in (c,d) correspond to initial SOD distribution in the TRIS buffer). The SOD is loaded into the crystals in the TRIS buffer at the protein concentration 1 mg/ml.

that for catalase (5×10^5 M). [68] Most probably, this can be explained by different affinity of proteins to the $CaCO_3$ surface. It is of note that study [68] also barely touched the question of the retention of protein activity after EDTA-mediated dissolution of vaterite cores. However, securing bio-activity under physiologically relevant conditions seems to be a crucial aspect for biomedical applications of $CaCO_3$-based delivery systems. Herein, further we focus on the retention of SOD activity after the co-synthesis and will make a specific focus on understanding of SOD release mechanism and kinetics in the solution simulating ionic strength of most of biological fluids (considered in the Section 3.4).

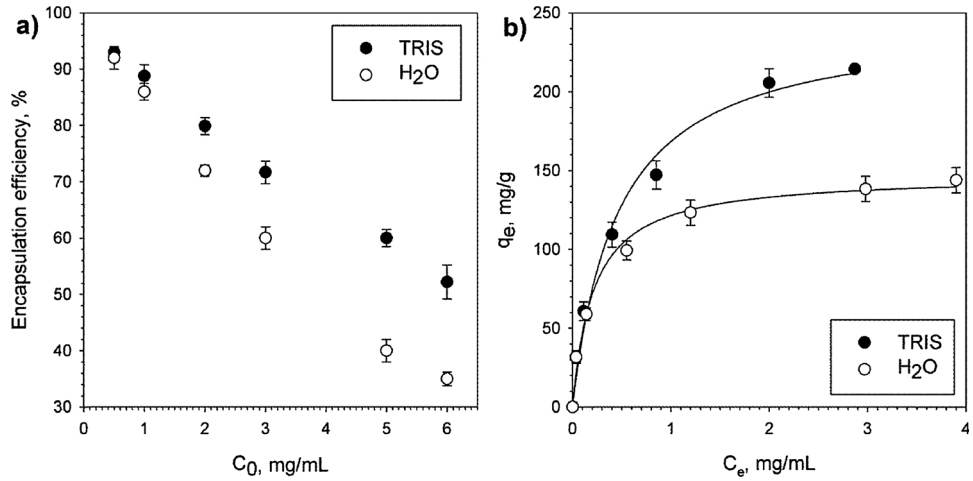

Fig. 6. (a) Efficiency of SOD adsorption depending on the initial SOD concentration, for microcrystals obtained in water and in the TRIS buffer. (b) Adsorption isotherms for SOD loading by co-synthesis in water and in the TRIS buffer (solid lines are the fitting curves according to parameters in Table 1).

Table 1
Thermodynamic parameters for SOD loading into vaterite crystals.

Crystal preparation	q_m, mg/g	K_a^{-1}, mg/ml	ΔG, kJ/mol
in water	150 ± 6	0.22 ± 0.01	−29 ± 1
in 60 mM TRIS	240 ± 8	0.37 ± 0.01	−29 ± 1

3.3. SOD activity retention after crystal dissolution

The study of the retention of the activity of SOD co-synthetized in this study under different conditions is of particular interest for SOD applications. First question to be faced is whether the SOD can retain its activity after dissolution of the crystals. This is important since the vaterite crystals are generally used as sacrificial templates to be eliminated (dissolved) for the formulation of polymer-based particles. According to conventional approaches, to study the retention of the SOD activity, vaterite microcrystals are dissolved using an equimolar amount of EDTA followed by the determination of the SOD activity by the indirect method based on the inhibition of the pyrogallol oxidation [73]. To obtain the activity retention, the SOD activity measured after crystal elimination was compared to that of SOD dissolved in water (taken as 100%). For SOD co-synthetized in the TRIS buffer, the retention of activity was found to be 48 ± 3%. This is 8 times higher than the activity for the enzyme co-synthetized in water (activity retention only 6 ± 2%). This demonstrates a significant increase in the retention of SOD activity for the crystal synthesis in the TRIS buffer as is likely due to a lower pH for the co-synthesis in the buffer compared to that in water.

A rather significant reduction of SOD activity for the synthesis in TRIS buffer (almost twice, activity retention 48 ± 3%) may be attributed to the effect of EDTA on the activity of the enzyme, whose active center includes copper. This phenomenon was also observed for other enzymes that have metal ions in their active center [70]. In order to better understand the reason of SOD activity reduction after crystal dissolution, the release of SOD from crystals and the activity of the released SOD have further been evaluated.

3.4. SOD release from crystals

The kinetics of the protein release from the crystals was studied in 150 mM NaCl solution in order to simulate ionic strength typical for most of biological fluids. The SOD release profile shows a burst (ca 30% released) within the first 10–20 min followed by a sustained release reaching the plateau at about 100 min of the release time (Fig. 7). Release profiles for the SOD co-synthetized in water and in the TRIS buffer are rather similar with a quicker release at the burst for the synthesis in the buffer. Interestingly, the release profiles reach a well-defined plateau (in about 100 min), however, this corresponds to the release of about 80–90% of the loaded enzyme. Most probably the equilibrium between soluble and adsorbed SOD is reached and therefore the complete release does not take place. Only after 24 h of incubation, the complete release has been observed (Fig. 7) that is explained by recrystallization of vaterite crystals to non-porous calcite and release of all SOD molecules out of the crystal pores (Fig. S2). The recrystallization of vaterite to calcite after 24 h of incubation was also confirmed by X-ray diffraction analysis (Fig. 3, bottom, c).

As a next step, the activity of the released SOD has been assessed. Fig. 8 shows the amount of the released SOD, the activity retention for the released SOD and SOD incubated in solution of 0.15 M NaCl for various time intervals. After almost 80% of the total loaded SOD has been released from crystals in 100 min incubation, the SOD activity retention was very high (about 85%). However, the enzymatic activity after 24 and 36 h of release has been significantly reduced giving the retained activity of about 50 and 30%, respectively. Similar trend in the reduction of the bioactivity for the SOD has been observed for the SOD

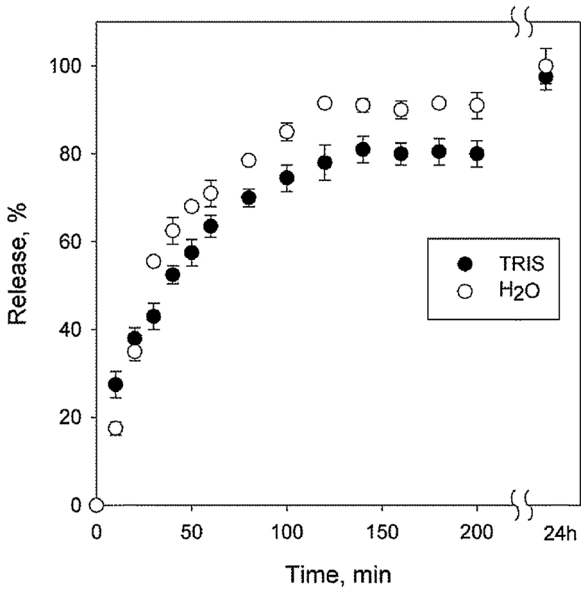

Fig. 7. Kinetics of SOD release in 150 mM NaCl from vaterite crystals synthetized in water and in the TRIS buffer.

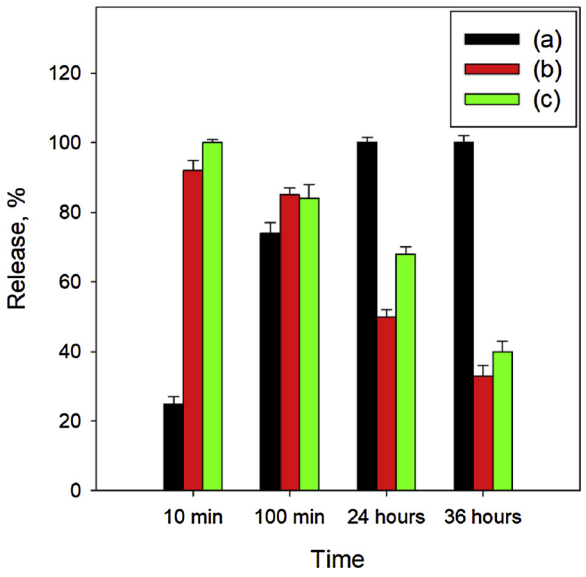

Fig. 8. The amount of SOD released from the crystals (a), the retention of enzymatic activity for SOD released from crystals in 150 mM NaCl (b) and for SOD solution in 150 mM NaCl stored for the same time as the release time (c). SOD synthesis is performed in the TRIS buffer using the SOD loading concentration 1 mg/ml.

solution in 0.15 M NaCl stored for the same period of time as for the release experiment (Fig. 7). This indicates that the SOD released at physiological ionic strength from the vaterite crystals keeps its bioactivity. However, long time storage of the enzyme in the presence of salt results in reduction of the bioactivity. This result supports the assumption that the presence of EDTA is most probably the reason of the reduction of the SOD activity after dissolution of the SOD-containing vaterite crystals (see the section above).

DLS investigation of the SOD size after the enzyme release from the crystals have been performed to examine whether the SOD molecules are aggregated or stay as single molecules. The aggregation would indicate the sticking of the molecules to each other as a result of unfolding due to a reduction of the bioactivity observed and described above. Fig. 5c,d show the intensity weighted distribution of

hydrodynamic diameters for SOD released from the crystals after 10 min and 24 h. The SOD molecules released after 10 min stay as single molecules (similar DLS profiles as for the SOD in water or in the TRIS buffer, Fig. 5a,c). However, the SOD molecules released from the crystals after 24 h possess a clear aggregation behavior as can be concluded from the well-defined shoulder on the DLS profile (Fig. 5d). This shows only a trend and one cannot conclude about the size of the aggregates formed, however, strong indicators of the aggregation of SOD molecules take place. Thus, the DLS results are in line with the observation of the reduction of SOD bioactivity. The activity reduction is a result of unfolding of the protein followed by enhancing the hydrophobicity of the protein surface and finally intermolecular protein aggregation.

3.5. Modeling the SOD release kinetics

The findings described above strongly indicate that the SOD is present in the crystals as aggregates but releases as single molecules keeping almost completely its bioactivity. To better understand the bimodal SOD release profile (Fig. 7) and to prove whether there is a link between the aggregated state of the enzyme in the crystals and the SOD release performance, a couple of release models have been applied to fit the results of the release experiments.

We propose that the release can be limited either by the rate of the dissolution of SOD aggregates inside the crystal pores or by the diffusion of single SOD molecules through the crystal pores. The experimental release data (Fig. 7) have been fitted by two release models corresponding to the above.

Bearing in mind that the concentration of SOD inside the microcrystals (ca 380 mg/ml) is much higher than SOD solubility in water, it was reasonable to assume above that SOD exists in the form of aggregates with compactly packed SOD molecules. The size of such aggregates cannot exceed the size of the crystal pores, so it is within a few tens of nm and thus a single aggregate should be made of tens to hundreds of SOD molecules at most. The dissolution of compactly packed structures like nanocrystals is generally described by the zero order reaction [76,77]. This is because the high surface area possessed by the nanocrystals (compared to the large crystals of μm-dimensions) results in a quick nanocrystal solvation and the increase in the concentration of the surrounding solution achieving a supersaturated state at the initial stage of the dissolution [78]. In this study, the SOD aggregates inside the crystals will behave similar to the nanocrystals described above due to the size of the aggregates and to describe the release kinetics, one can apply the zero-order kinetical equation:

$$q_{\max} - q_t = kt \tag{3}$$

where q_t and $q_{\max}$ – cumulative amount of SOD released at time t and the maximum released amount, respectively, (mg/g); k – release rate constant, (mg/g/min).

From the other hand, the model proposed by Baker and Lonsdale can also be applied for our case. This model describes the release kinetics of the drug (SOD) that is encapsulated into the matrices of a spherical shape (vaterite $CaCO_3$) and is loaded into extremely high concentrations (above solubility) as follows the equation:

$$\frac{3}{2}\left[1 - (1 - \frac{q_t}{q_{\max}})^{\frac{2}{3}}\right] - \frac{q_t}{q_{\max}} = \frac{3Dc_s}{R^2 c_0}t = k_{B-L}t \tag{4}$$

D – effective diffusion coefficient of SOD within the vaterite microcrystal; R – radius of the $CaCO_3$ crystal; c_s – SOD solubility; c_0 – SOD initial concentration of SOD loaded into the crystal; $k_{B\text{-}L}$ – constant.

Zero-order kinetics is applicable for initial stages of the release and has been used for the first ca 50% of SOD release and the Baker and Lonsdale model has assumed the maximum release as per the plateau well-defined after ca 140 min of release (Fig. 9).

The mathematical fitting of these two models to the SOD release kinetics is shown in Fig. 9; parameters of the fitting are summarized in Table S1. The release of SOD co-synthetized in water and in the TRIS buffer is well-fitted to the Baker-Lonsdale model (R^2 0.99) indicating a dominant role of SOD molecular diffusion through crystal pores. In the case of co-synthesis in the TRIS buffer, the dissolution of the SOD aggregates does not play a role on the initial stage of the release (as indicated by rather low R^2 of 0.83) and the overall release mechanism depends solely on the diffusion limitations (Fig. 9a). On the contrary, in the case of the co-synthesis in water, the first part of the release curve (Fig. 9b) is well-fitted to the zero-order dissolution kinetics with R^2 0.98. This allows one to propose that both, SOD aggregate dissolution and SOD diffusion through the pores make an impact to the release kinetics. However, considered together, these results point to the higher stability of SOD aggregates formed for the synthesis in water compared to the aggregates formed for the synthesis in the TRIS buffer.

This can be caused by stronger unfolding of the SOD molecules at higher pH (for co-synthesis in water) leading to stronger intermolecular SOD-SOD interactions facilitating aggregation. However, the size of the aggregates is most probably larger for the co-synthesis in TRIS buffer since the SOD content is 1.6 times higher than that for the co-synthesis in water (Table 1). So, one can speculate that not a size of aggregates of the protein but the strength of the aggregation will define the protein release kinetics. Based on the findings described in this section and above, the following section below will focus on the loading/release mechanism of SOD.

3.6. Mechanism of SOD loading and release

Based on the results of this study, one can propose the mechanism of SOD loading into the vaterite crystals and SOD release from the crystals. Fig. 10 shows the schematics of these processes. SOD molecules are first aggregated being in the solution of $CaCl_2$ (Fig. 10a). Mixing the solution of SOD in $CaCl_2$ and solution of Na_2CO_3 together under an intensive stirring results in growth of vaterite crystals made of small nanocrystallines (typical size tens of nm [49]) as building blocks with the pores formed in between the nanocrystallines (Fig. 10a–b). The SOD aggregates are trapped into the crystal pores. Moreover, due to a very high content of the SOD co-synthetized in the crystals (the internal concentration is about 380 mg/ml that is roughly a third of the SOD concentration in a pure solid SOD), the SOD is rather compactly packed into the pores being in the aggregated state. In the physiologically relevant ionic strength (150 mM NaCl), the SOD is released from the crystals keeping its bioactivity and the release kinetics is driven the diffusion of dissociated single SOD molecules through the crystal pores (Fig. 10b–c). The complete release of SOD takes place after recrystallization of the vaterite crystals into non-porous calcite and is driven by exclusion of SOD molecules from the internal volume of the crystals upon significant reduction of the crystal porosity. Thus, the SOD release can be of a prolonged character due to rather slow diffusion through the crystal pores and can be completed (release of all loaded content) due to the recrystallization phenomenon.

3.7. Perspectives for ophthalmology

Despite the fairly large number of experimental studies on the use of SOD for the treatment of various eye diseases, drugs based on it do not yet exist. The only exception is the drug Erisod (later renamed Rexod-OF). There is a patented method of treatment of open angle glaucoma with this drug [79]. The treatment regimen is rather complicated and consists of 6-fold instillations of the SOD solution every 5 min for half an hour. In experimental studies of the treatment of other eye diseases using SOD (eye burns, corneal ulcers, uveitis), complex drug administration schemes, including daily multiple (5–6 times a day) instillation of SOD solution [25,80,81] or subconjunctival injections [23] have also been used.

It is obvious that such complex schemes are designed to prolong the

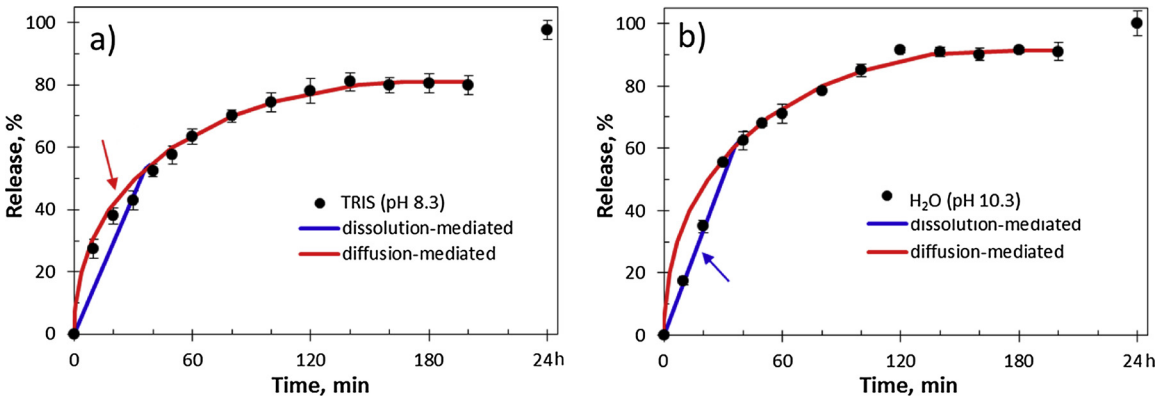

Fig. 9. SOD release kinetics in 150 mM NaCl from $CaCO_3$ microcrystals obtained by co-synthesis in TRIS buffer (a) and in water (b). Mathematical fitting of release kinetics has been performed using two models: zero order kinetics (dissolution-mediated) and Baker-Lonsdale model (diffusion-mediated). Arrows indicate better fitting for burst release within first 40 min.

therapeutic effect of SOD due to imperfection of the instillation route for drugs administered, as already mentioned in the introduction, as well as the rapid SOD elimination. Undoubtedly, the use of various delivery systems would significantly simplify the treatment regimen, as well as increase its effectiveness. However, the delivery systems currently described in the literature have a number of significant disadvantages. Thus, pegylation of SOD significantly lowers the permeability of the enzyme through the microvessels to the area of damage [82]. In addition, pegylation of SOD leads to the formation of heterogeneous products due to a large number of available amino groups on the surface of the enzyme, which significantly affects the biodistribution and circulation times of the PEG-SOD complex in the body, as well as its antigenic and immunogenic properties [83]. The use of liposomes as carriers [21] also has disadvantages due to their instability (half-life of 4.2 h) and potential toxicity [84,85]. The use of biodegradable and biocompatible polylactoglycolic (PLG) particles based on copolymer D, L-lactide-glycol [17] leads to the fact that the PLG-matrix makes it difficult for the substrate to access the active center of the enzyme, and the hydrolysis of polylactoglycol can quickly deactivate enzymes in the matrix [86]. The use of nanoparticles based on complexes of enzymes and block copolymers [18,87] may be economically unprofitable due to the high cost of copolymers and low SOD retained activity.

Recently, successful utilization of SOD (free enzyme and its conjugate with poly(L-lysine)-poly(ethyleneglycol) copolymer) has been reported for the treatment of eye inflammation in rabbits. Significant elimination of the inflammatory signs in the eye has been demonstrated by multiple biochemical and histological analysis [88].

Against this background, the vaterite calcium carbonate crystals can

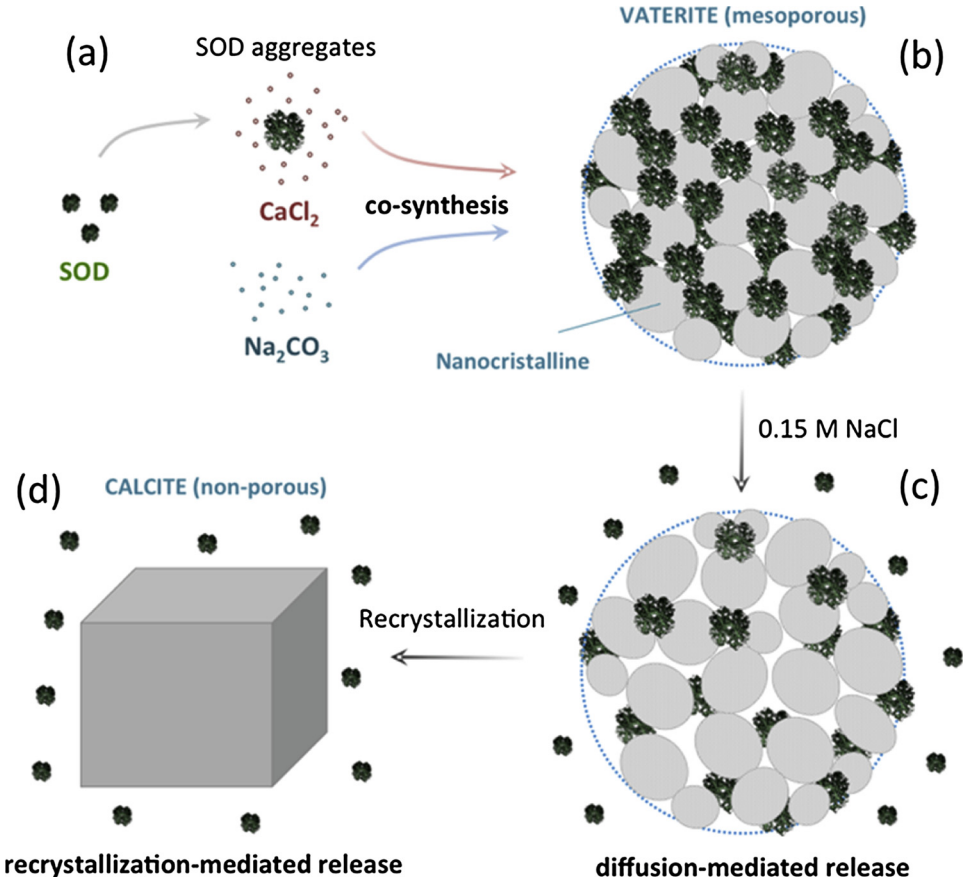

Fig. 10. Schematics of the co-synthesis of SOD-containing vaterite crystals via mixing of SOD molecules with $CaCl_2$ and Na_2CO_3 (a–b). The aggregation of SOD in $CaCl_2$ results in the integration of SOD aggregates into the crystals made of nanocrystallines as building blocks that provides the mesoporous crystal architecture (b). Single SOD molecules are released from the crystal in 150 mM NaCl showing a partial release (b–c). The complete release of SOD takes place after recrystallization of the porous vaterite into non-porous calcite (c–d) that is accompanied by a dramatic reduction in the crystal porosity and, as a result, the reduction in the hosting capability for SOD.

be an excellent alternative system for drug delivery to the eye. On the one hand, the synthesis of such particles is extremely simple, and the initial components are inexpensive. On the other hand, calcium carbonate is completely biocompatible and biodegradable and potentially does not possess toxic, immunogenic or any other negative responses. Thus, in preliminary experiments, we showed that injection of vaterite microcrystals into the eyes of rabbits at a concentration of 10 mg/ml did not cause any negative reaction (data not shown). This indicates a high promise of vaterite crystals for ocular drug delivery. The *in vivo* study on the SOD delivery into eyes via the vaterite crystals as drug delivery vectors is in the focus of our upcoming research.

4. Conclusions

This study shows that SOD can effectively be loaded into $CaCO_3$ vaterite crystals giving extremely high content in the crystals reaching a concentration of up to 380 mg/ml (10^{-2} M). This is driven by Ca^{2+}-mediated aggregation of SOD molecules to be embedded into the vaterite crystals during the co-synthesis. Synthesis of the crystals in TRIS buffer at pH 8.4 is proven to be advantageous compared to the synthesis in water (pH 10.3) because it allows to preserve enzymatic activity of SOD while crystal morphology remains unaffected. SOD releasing from the crystals at physiologically relevant ionic strength can keep almost all its bioactivity during ca. 24 h under release conditions. The release kinetics of SOD is governed by both the dissolution of SOD aggregates and by the diffusion of SOD thorough the crystal pores. At the same time, the contribution of the aggregate dissolution is higher for the co-synthesis in water as may be explained by stronger SOD-SOD interactions for protein molecules unfolded at higher pH for the synthesis in water. The complete release of SOD is governed by the recrystallization of porous vaterite crystals into more thermodynamically stable non-porous calcite polymorph form. The mild aggregation of the SOD upon co-synthesis demonstrated in this work allows to keep the enzyme bioactive that is one of the most important criterion for SOD bio-applications. The extremely high content of SOD into the crystals makes the crystals very attractive for therapeutic formulations with prolonged release, also for ophthalmological purposes. The latter is supported by first *in vivo* experiments performed with rabbits and indicating no inflammation or other reaction caused by the crystals after administration into eyes.

Author contributions

The manuscript was written through contributions of all authors. All authors have given approval to the final version of the manuscript.

Acknowledgments

The work was performed within the framework of the M.V. Lomonosov Moscow State University state task, part 2 (government grant AAAA-A16-116052010081-5). This work was supported in part by M.V. Lomonosov Moscow State University Program of Development. D.V. acknowledges QR Fund 2018-2019 from Nottingham Trent University. A.V. thanks the Europeans Union's Horizon 2020 research and innovation programme for funding (the Marie-Curie Individual Fellowship LIGHTOPLEX-747245).

Appendix A. Supplementary data

Supplementary material related to this article can be found, in the online version, at doi:https://doi.org/10.1016/j.colsurfb.2019.05.077.

References

[1] D. Achouri, K. Alhanout, P. Piccerelle, V. Andrieu, Recent advances in ocular drug delivery, Drug Dev. Ind. Pharm. 39 (11) (2013) 1599–1617.
[2] L. Rabinovich-Guilatt, P. Couvreur, G. Lambert, C. Dubernet, Cationic vectors in ocular drug delivery, J. Drug Target. 12 (9–10) (2004) 623–633.
[3] D.R. Gaikwad, D.M. Sakarkar, P.R. Kamble, G.R. Ghuge, K.P. Hattiambire, Recent advances in ocular drug delivery systems, Indo Am. J. Pharm. Res. 3 (4) (2013) 3216–3232.
[4] K.M. Saari, L. Nelimarkka, V. Ahola, T. Loftsson, E. Stefánsson, Comparison of topical 0.7% dexamethasone-cyclodextrin with 0.1% dexamethasone sodium phosphate for postcataract inflammation, Graefe's Arch. Clin. Exp. Ophthalmol. 244 (5) (2006) 620–626.
[5] H. Sasaki, Y. Igarashi, T. Nagano, K. Nishida, J. Nakamura, Different effects of absorption promoters on corneal and conjunctival penetration of ophthalmic beta-blockers, Pharm. Res. 12 (8) (1995) 1146–1150.
[6] A. Ludwig, The use of mucoadhesive polymers in ocular drug delivery, Adv. Drug Deliv. Rev. 57 (11) (2005) 1595–1639.
[7] Y. Shen, J. Tu, Preparation and ocular pharmacokinetics of ganciclovir liposomes, AAPS J. 9 (3) (2007) E371–E377.
[8] S.K. Sahoo, F. Dilnawaz, S. Krishnakumar, Nanotechnology in ocular drug delivery, Drug Discov. Today 13 (3-4) (2008) 144–151.
[9] P.W. Morrison, V.V. Khutoryanskiy, Advances in ophthalmic drug delivery, Ther. Deliv. 5 (12) (2014) 1297–1315.
[10] Y.C. Kim, B. Chiang, X. Wu, M.R. Prausnitz, Ocular delivery of macromolecules, J. Control. Release 190 (2014) 172–181.
[11] K. Yasui, A. Baba, Therapeutic potential of superoxide dismutase (SOD) for resolution of inflammation, Inflamm. Res. 55 (9) (2006) 359–363.
[12] Y. Mizushima, K. Hoshi, A. Yanagawa, K. Takano, Topical application of superoxide dismutase cream, Drugs Exp. Clin. Res. 17 (2) (1991) 127–131.
[13] K. Vorauer-Uhl, E. Fürnschlief, A. Wagner, B. Ferko, H. Katinger, Topically applied liposome encapsulated superoxide dismutase reduces postburn wound size and edema formation, Eur. J. Pharm. Sci. 14 (1) (2001) 63–67.
[14] I.V. Churilova, E.V. Zinov'ev, B.A. Paramonov, Y.I. Drozdova, V.O. Sidel'nikov, V.Yu Chebotarev, Effect of Erysod (erythrocyte superoxide dismutase) on blood concentration of reactive oxygen species in patients with severe burns and burn shock, Bull. Exp. Biol. Med. 134 (5) (2002) 454–456.
[15] M.K. Reddy, L. Wu, W. Kou, A. Ghorpade, V. Labhasetwar, Superoxide dismutase-loaded PLGA nanoparticles protect cultured human neurons under oxidative stress, Appl. Biochem. Biotechnol. 151 (2-3) (2008) 565–577.
[16] M. Hangaishi, H. Nakajima, J. Taguchi, R. Igarashi, J. Hoshino, K. Kurokawa, S. Kimura, R. Nagai, M. Ohno, Lecithinized Cu, Zn-superoxide dismutase limits the infarct size following ischemia-reperfusion injury in rat hearts in vivo, Biochem. Biophys. Res. Commun. 285 (5) (2001) 1220–1225.
[17] M.K. Reddy, V. Labhasetwar, Nanoparticle-mediated delivery of superoxide dismutase to the brain: an effective strategy to reduce ischemia-reperfusion injury, FASEB J. 23 (5) (2009) 1384–1395.
[18] D.S. Manickam, A.M. Brynskikh, J.L. Kopanic, P.L. Sorgen, N.L. Klyachko, E.V. Batrakova, T.K. Bronich, A.V. Kabanov, Well-defined cross-linked antioxidant nanozymes for treatment of ischemic brain injury, J. Control. Release 162 (3) (2012) 636–645.
[19] E.G. Rosenbaugh, J.W. Roat, L. Gao, R.-F. Yang, D.S. Manickam, J.X. Yin, H.D. Schultz, T.K. Bronich, E.V. Batrakova, A.V. Kabanov, I.H. Zucker, M.C. Zimmerman, The attenuation of central angiotensin II-dependent pressor response and intra-neuronal signaling by intracarotid injection of nanoformulated copper/zinc superoxide dismutase, Biomaterials 31 (19) (2010) 5218–5226.
[20] S. Giovagnoli, G. Luca, I. Casaburi, P. Blasi, G. Macchiarulo, M. Ricci, M. Calvitti, G. Basta, R. Calafiore, C. Rossi, Long-term delivery of superoxide dismutase and catalase entrapped in poly(lactide-co-glycolide) microspheres: in vitro effects on isolated neonatal porcine pancreatic cell clusters, J. Control. Release 107 (1) (2005) 65–77.
[21] L.M. Corvo, J.C. Jorge, R. Van't Hof, M.E. Cruz, D.J. Crommelin, G. Storm, Superoxide dismutase entrapped in long-circulating liposomes: formulation design and therapeutic activity in rat adjuvant arthritis, Biochim. Biophys. Acta 1564 (1) (2002) 227–236.
[22] N.A. Rao, A.J. Calandra, A. Sevanian, B. Bowe, J.M. Delmage, G.E. Marak Jr., Modulation of lens-induced uveitis by superoxide dismutase, Ophthalmic Res. 18 (1) (1986) 41–46.
[23] M. Yamada, H. Shichi, T. Yuasa, Y. Tanouchi, Y. Mimura, Superoxide in ocular inflammation: human and experimental uveitis, J. Free Radic. Biol. Med. 2 (2) (1986) 111–117.
[24] V.S. Nirankari, S.D. Varma, V. Lakhanpal, R.D. Richards, Superoxide radical scavenging agents in treatment of alkali burns. An experimental study, Arch. Ophthalmol. 99 (5) (1981) 886–887.
[25] J.L. Alio, M.J. Ayala, M.E. Mulet, A. Artola, J.M. Ruiz, J. Bellot, Antioxidant therapy in the treatment of experimental acute corneal inflammation, Ophthalmic Res. 27 (3) (1995) 136–143.
[26] Y. de Kozak, J.P. Nordman, J.P. Faure, N.A. Rao, G.E. Marak Jr., Effect of antioxidant enzymes on experimental uveitis in rats, Ophthalmic Res. 21 (3) (1989) 230–234.
[27] N.A. Rao, A. Sevanian, M.A. Fernandez, J.L. Romero, J.P. Faure, Y. de Kozak, G.O. Till, G.E. Marak Jr., Role of oxygen radicals in experimental allergic uveitis, Invest. Ophthalmol. Vis. Sci. 28 (5) (1987) 886–892.
[28] C. Regnault, M. Soursac, M. Roch-Arveiller, E. Postaire, G. Hazebroucq, Pharmacokinetics of superoxide dismutase in rats after oral administration, Biopharm. Drug Dispos. 17 (2) (1996) 165–174.
[29] B. Odlind, L.E. Appelgren, A. Bayati, M. Wolgast, Tissue distribution of 125I-labelled bovine superoxide dismutase (SOD) in the rat, Pharmacol. Toxicol. 62 (2) (1988) 95–100.
[30] A. Bayati, O. Källskog, B. Odlind, M. Wolgast, Plasma elimination kinetics and renal

handling of copper/zinc superoxide dismutase in the rat, Acta Physiol. Scand. 134 (1) (1988) 65–74.
[31] F.M. Veronese, P. Caliceti, O. Schiavon, M. Sergi, Polyethylene glycol-superoxide dismutase, a conjugate in search of exploitation, Adv. Drug Deliv. Rev. 54 (4) (2002) 587–606.
[32] T. Ishihara, S. Nara, T. Mizushima, Interactions of lecithinized superoxide dismutase with serum proteins and cells, J. Pharm. Sci. 103 (7) (2014) 1987–1994.
[33] R. Galović Rengel, K. Barisić, Z. Pavelić, T. Zanić Grubisić, I. Cepelak, J. Filipović-Grcić, High efficiency entrapment of superoxide dismutase into mucoadhesive chitosan-coated liposomes, Eur. J. Pharm. Sci. 15 (5) (2002) 441–448.
[34] S. Giovagnoli, P. Blasi, M. Ricci, C. Rossi, Biodegradable microspheres as carriers for native superoxide dismutase and catalase delivery, AAPS PharmSciTech 5 (4) (2004) e51.
[35] O. Celik, J. Akbuğa, Preparation of superoxide dismutase loaded chitosan microspheres: characterization and release studies, Eur. J. Pharm. Biopharm. 66 (1) (2007) 42–47.
[36] N. Sudareva, O. Suvorova, N. Saprykina, A. Vilesov, P. Bel'tyukov, S. Petunov, Alginate-containing systems for oral delivery of superoxide dismutase. Comparison of various configurations and their properties, J. Microencapsul. 33 (5) (2016) 487–496.
[37] C.-Y. He, Z.-P. Liang, C.-Y. Wang, X.-X. Liu, Z. Tong, Immobilization of superoxide dismutase by layer-by-layer assembly on surface of PS colloid particles and their bioactivity, Chem. J. Chin. Univ. 26 (1) (2005) 88–92.
[38] D.V. Volodkin, N.I. Larionova, G.B. Sukhorukov, Protein encapsulation via porous $CaCO_3$ microparticles templating, Biomacromolecules 5 (5) (2004) 1962–1972.
[39] D.V. Volodkin, A.I. Petrov, M. Prevot, G.B. Sukhorukov, Matrix polyelectrolyte microcapsules: new system for macromolecule encapsulation, Langmuir 20 (8) (2004) 3398–3406.
[40] Y.-H. Won, H.S. Jang, D.-W. Chung, L.A. Stanciu, Multifunctional calcium carbonate microparticles: synthesis and biological applications, J. Mater. Chem. 20 (36) (2010) 7728–7733.
[41] S. Biradar, P. Ravichandran, R. Gopikrishnan, V. Goornavar, J.C. Hall, V. Ramesh, S. Baluchamy, R.B. Jeffers, G.T. Ramesh, Calcium carbonate nanoparticles: synthesis, characterization and biocompatibility, J. Nanosci. Nanotechnol. 11 (8) (2011) 6868–6874.
[42] N.G. Balabushevich, V.A. Izumrudov, N.I. Larionova, Protein microparticles with controlled stability prepared via layer-by-layer adsorption of biopolyelectrolytes, Polym. Sci. Ser. A 54 (7) (2012) 540–551.
[43] D. Volodkin, $CaCO_3$ templated micro-beads and -capsules for bioapplications, Adv. Colloid Interface Sci. 207 (2014) 306–324.
[44] S. Maleki Dizaj, M. Barzegar-Jalali, M.H. Zarrintan, K. Adibkia, F. Lotfipour, Calcium carbonate nanoparticles as cancer drug delivery system, Expert Opin. Drug Deliv. 12 (10) (2015) 1649–1660.
[45] E.A. Genina, Y.I. Svenskaya, I.Y. Yanina, L.E. Dolotov, N.A. Navolokin, A.N. Bashkatov, G.S. Terentyuk, A.B. Bucharskaya, G.N. Maslyakova, D.A. Gorin, V.V. Tuchin, G.B. Sukhorukov, In vivo optical monitoring of transcutaneous delivery of calcium carbonate microcontainers, Biomed. Opt. Express 7 (6) (2016) 2082–2087.
[46] R. Roth, J. Schoelkopf, J. Huwyler, M. Puchkov, Functionalized calcium carbonate microparticles for the delivery of proteins, Eur. J. Pharm. Biopharm. 122 (2018) 96–103.
[47] A.D. Trofimov, A.A. Ivanova, M.V. Zyuzin, A.S. Timin, Porous inorganic carriers based on silica, calcium carbonate and calcium phosphate for controlled/modulated drug delivery: fresh outlook and future perspectives, Pharmaceutics 10 (4) (2018) E167.
[48] B.V. Parakhonskiy, A.M. Yashchenok, S. Donatan, D.V. Volodkin, F. Tessarolo, R. Antolini, H. Möhwald, A.G. Skirtach, Macromolecule loading into spherical, elliptical, star-like and cubic calcium carbonate carriers, ChemPhysChem 15 (13) (2014) 2817–2822.
[49] N. Feoktistova, J. Rose, V.Z. Prokopović, A.S. Vikulina, A. Skirtach, D. Volodkin, Controlling the vaterite $CaCO_3$ crystal pores. Design of tailor-made polymer based microcapsules by hard templating, Langmuir 32 (17) (2016) 4229–4238.
[50] S. Schmidt, K. Uhlig, C. Duschl, D. Volodkin, Stability and cell uptake of calcium carbonate templated insulin microparticles, Acta Biomater. 10 (3) (2014) 1423–1430.
[51] T. Paulraj, N. Feoktistova, N. Velk, K. Uhlig, C. Duschl, D. Volodkin, Microporous polymeric 3D scaffolds templated by the layer-by-layer self-assembly, Macromol. Rapid Commun. 35 (16) (2014) 1408–1413.
[52] S. Schmidt, M. Behra, K. Uhlig, N. Madaboosi, L. Hartmann, C. Duschl, D. Volodkin, Mesoporous protein particles through colloidal CaCO3 templates, Adv. Funct. Mater. 23 (1) (2013) 116–123.
[53] I.Y. Stetciura, A.V. Markin, A.N. Ponomarev, A.V. Yakimansky, T.S. Demina, C. Grandfils, D.V. Volodkin, D.A. Gorin, New surface-enhanced Raman scattering platforms: composite calcium carbonate microspheres coated with astralen and silver nanoparticles, Langmuir 29 (12) (2013) 4140–4147.
[54] I.Y. Stetciura, A. Yashchenok, A. Masic, E.V. Lyubin, O.A. Inozemtseva, M.G. Drozdova, E.A. Markvichova, B.N. Khlebtsov, A.A. Fedyanin, G.B. Sukhorukov, D.A. Gorin, D. Volodkin, Composite SERS-based satellites navigated by optical tweezers for single cell analysis, Analyst 140 (15) (2015) 4981–4986.
[55] A. Sergeeva, R. Sergeev, E. Lengert, A. Zakharevich, B. Parakhonskiy, D. Gorin, S. Sergeev, D. Volodkin, Composite magnetite and protein containing CaCO3 crystals. External manipulation and vaterite → calcite recrystallization-mediated release performance, ACS Appl. Mater. Interfaces 7 (38) (2015) 21315–22125.
[56] L. Jeannot, M. Bell, R. Ashwell, D. Volodkin, A.S. Vikulina, Internal structure of matrix-type multilayer capsules templated on porous vaterite $CaCO_3$ crystals as probed by staining with a fluorescence dye, Micromachines 9 (11) (2018) 547.
[57] M. Behra, S. Schmidt, J. Hartmann, D.V. Volodkin, L. Hartmann, Synthesis of porous PEG microgels using CaCO3 microspheres as hard templates, Macromol. Rapid Commun. 33 (12) (2012) 1049–1054.
[58] N. Feoktistova, G. Stoychev, N. Puretskiy, L. Ionov, D. Volodkin, Porous thermoresponsive pNIPAM microgels, Eur. Polym. J. 68 (2015) 650–656.
[59] A.S. Sergeeva, D.A. Gorin, D.V. Volodkin, In-situ assembly of Ca-alginate gels with controlled pore loading/release capability, Langmuir 31 (39) (2015) 10813–10821.
[60] A. Sergeeva, N. Feoktistova, V. Prokopovic, D. Gorin, D. Volodkin, Design of porous alginate hydrogels by sacrificial $CaCO_3$ templates: pore formation mechanism, Adv. Mater. Interfaces 2 (18) (2015) 1500386.
[61] M. Fujiwara, K. Shiokawa, M. Araki, N. Ashitaka, K. Morigaki, T. Kubota, Y. Nakahara, Encapsulation of proteins into CaCO3 by phase transition from vaterite to calcite, Cryst. Growth Des. 10 (9) (2010) 4030–4037.
[62] S. Chen, D. Zhao, F. Li, R.-X. Zhuo, S.-X. Cheng, Co-delivery of genes and drugs with nanostructured calcium carbonate for cancer therapy, RSC Adv. 2 (5) (2012) 1820–1826.
[63] K. Sato, M. Seno, J.-I. Anzai, Release of insulin from calcium carbonate microspheres with and without layer-by-layer thin coatings, Polymers 6 (8) (2014) 2157–2165.
[64] L.N. Hassani, F. Hindré, T. Beuvier, B. Calvignac, N. Lautram, A. Gibaud, F. Boury, Lysozyme encapsulation into nanostructured $CaCO_3$ microparticles using a supercritical CO_2 process and comparison with the normal route, J. Mater. Chem. B 1 (32) (2013) 4011–4019.
[65] N. Sudareva, H. Popova, N. Saprykina, S. Bronnikov, Structural optimization of calcium carbonate cores as templates for protein encapsulation, J. Microencapsul. 31 (4) (2014) 333–343.
[66] C.-Q. Wang, M.-Q. Gong, J.-L. Wu, R.-X. Zhuo, S.-X. Cheng, Dual-functionalized calcium carbonate based gene delivery system for efficient gene delivery, RSC Adv. 4 (73) (2014) 38623–38629.
[67] N.G. Balabushevich, A.V. Lopes de Guerenu, N.A. Feoktistova, D. Volodkin, Protein loading into porous $CaCO_3$ microspheres: adsorption equilibrium and bioactivity retention, Phys. Chem. Chem. Phys. 17 (4) (2015) 2523–2530.
[68] A.S. Vikulina, N.A. Feoktistova, N.G. Balabushevich, A.G. Skirtach, D.V. Volodkin, The mechanism of catalase loading into porous vaterite $CaCO_3$ crystals by co-synthesis, Phys. Chem. Chem. Phys. 20 (13) (2018) 8822–8831.
[69] N.G. Balabushevich, E.A. Sholina, E.V. Mikhalchik, L.Y. Filatova, A.S. Vikulina, D. Volodkin, Self-assembled mucin-containing microcarriers via hard templating on $CaCO_3$ crystals, Micromachines 9 (6) (2018) E307.
[70] N.G. Balabushevich, A.V. Lopez de Guerenu, N.A. Feoktistova, D. Volodkin, Protein-containing multilayer capsules by templating on mesoporous $CaCO_3$ particles: post- and pre-loading approaches, Macromol. Biosci. 16 (1) (2016) 95–105.
[71] N.G. Balabushevich, E.A. Kovalenko, E.V. Mikhalchik, L.Y. Filatova, D. Volodkin, A.S. Vikulina, Mucin adsorption on vaterite $CaCO_3$ microcrystals for the prediction of mucoadhesive properties, J. Colloid Interface Sci. 545 (2019) 330–339.
[72] M.M. Bradford, A rapid and sensitive method for the quantitation of microgram quantities of protein utilizing the principle of protein-dye binding, Anal. Biochem. 72 (1-2) (1976) 248–254.
[73] X. Yi, M.C. Zimmerman, R. Yang, J. Tong, S. Vinogradov, A.V. Kabanov, Pluronic-modified superoxide dismutase 1 attenuates angiotensin II-induced increase in intracellular superoxide in neurons, Free Radic. Biol. Med. 49 (4) (2010) 548–558.
[74] S.S. Leal, I. Cardoso, J.S. Valentine, C.M. Gomes, Calcium ions promote superoxide dismutase 1 (SOD1) aggregation into non-fibrillar amyloid: a link to toxic effects of calcium overload in amyotrophic lateral sclerosis (ALS)? J. Biol. Chem. 288 (35) (2013) 25219–25228.
[75] J. Plank, G. Bassioni, Adsorption of carboxylate anions on a $CaCO_3$ surface, Z. Naturforsch. 62 (10) (2007) 1277–1284.
[76] T. Gülsün, R.N. Gürsoy, L. Öner, Nanocrystal technology for oral delivery of poorly water-soluble drugs, FABAD J. Pharm. Sci. 34 (1) (2009) 55–65.
[77] M. Guo, Y. Dong, Y. Wang, M. Ma, Z. He, Q. Fu, Fabrication, characterization, stability and in vitro evaluation of nitrendipine nanocrystals by media milling, Powder Technol. (2018), https://doi.org/10.1016/j.powtec.2018.08.018.
[78] J. Sun, F. Wang, Y. Sui, Z. She, W. Zhai, C. Wang, Y. Deng, Effect of particle size on solubility, dissolution rate, and oral bioavailability: evaluation using coenzyme Q_{10} as naked nanocrystals, Int. J. Nanomed. 7 (2012) 5733–5744.
[79] V.N. Alekseev, E.B. Martynova, I.V. Churilova, Method for Treating Primary Open Angle Glaucoma. RU2144343 (C1), January 20, 2000.
[80] K. Matsumoto, S. Shimmura, E. Goto, K. Saito, T. Takeuchi, S. Miyajima, A. Negi, K. Tsubota, Lecithin-bound superoxide dismutase in the prevention of neutrophil-induced damage of corneal tissue, Invest. Ophthalmol. Vis. Sci. 39 (1) (1998) 30–35.
[81] S. Shimmura, R. Igarashi, H. Yaguchi, Y. Ohashi, J. Shimazaki, K. Tsubota, Lecithin-bound superoxide dismutase in the treatment of noninfectious corneal ulcers, Am. J. Ophthalmol. 135 (5) (2003) 613–619.
[82] J.W. Francis, J. Ren, L. Warren, R.H.Jr. Brown, S.P. Finklestein, Postischemic infusion of Cu/Zn superoxide dismutase or SOD: Tet451 reduces cerebral infarction following focal ischemia/reperfusion in rats, Exp. Neurol. 146 (2) (1997) 435–443.
[83] K. Knop, R. Hoogenboom, D. Fischer, U.S. Schubert, Poly(ethylene glycol) in drug delivery: pros and cons as well as potential alternatives, Angew. Chem. Int. Ed. Engl. 49 (36) (2010) 6288–6308.
[84] S. Imaizumi, V. Woolworth, R.A. Fishman, P.H. Chan, Liposome-entrapped superoxide dismutase reduces cerebral infarction in cerebral ischemia in rats, Stroke 21 (9) (1990) 1312–1317.
[85] J. Sinha, N. Das, M.K. Basu, Liposomal antioxidants in combating ischemia-reperfusion injury in rat brain, Biomed. Pharmacother. 55 (5) (2001) 264–271.
[86] W. Jiang, S.P. Schwendeman, Stabilization of tetanus toxoid encapsulated in PLGA

microspheres, Mol. Pharm. 5 (5) (2008) 808–817.
[87] N.L. Klyachko, D.S. Manickam, A.M. Brynskikh, S.V. Uglanova, S. Li, S.M. Higginbotham, T.K. Bronich, E.V. Batrakova, A.V. Kabanov, Cross-linked antioxidant nanozymes for improved delivery to CNS, Nanomedicine 8 (1) (2012) 119–129.
[88] O.A. Kost, O.V. Beznos, N.G. Davydova, D.S. Manickam, I.I. Nikolskaya, A.E. Guller, P.V. Binevski, N.B. Chesnokova, A.B. Shekhter, N.L. Klyachko, A.V. Kabanov, Superoxide dismutase 1 nanozyme for treatment of eye inflammation, Oxid. Med. Cell. Longev. 2015 (2015) 5194239.